



저작자표시 2.0 대한민국

이용자는 아래의 조건을 따르는 경우에 한하여 자유롭게

- 이 저작물을 복제, 배포, 전송, 전시, 공연 및 방송할 수 있습니다.
- 이차적 저작물을 작성할 수 있습니다.
- 이 저작물을 영리 목적으로 이용할 수 있습니다.

다음과 같은 조건을 따라야 합니다:



저작자표시. 귀하는 원저작자를 표시하여야 합니다.

- 귀하는, 이 저작물의 재이용이나 배포의 경우, 이 저작물에 적용된 이용허락조건을 명확하게 나타내어야 합니다.
- 저작권자로부터 별도의 허가를 받으면 이러한 조건들은 적용되지 않습니다.

저작권법에 따른 이용자의 권리는 위의 내용에 의하여 영향을 받지 않습니다.

이것은 [이용허락규약\(Legal Code\)](#)을 이해하기 쉽게 요약한 것입니다.

[Disclaimer](#) 

석사학위논문

Protective Roles of
PBN and GKT136901 in METH
-Induced BBB Dysfunction

계명대학교 대학원
의학과

황종수

지도교수 서지혜

2020년 8월

Protective Roles of PBN and GKT136901 in METH -Induced BBB Dysfunction

지도교수 서 지 혜

이 논문을 석사학위 논문으로 제출함

2 0 2 0 년 8 월

계 명 대 학 교 대 학 원

의 학 과

황 중 수

황종수의 석사학위 논문을 인준함

주 심 하 은 영

부 심 서 지 혜

부 심 박 병 덕

계 명 대 학 교 대 학 원

2 0 2 0 년 8 월

Acknowledgement

본 논문이 제출되기까지 바쁘신 일정에도 밤낮 없이 논문의 교정, 심사까지 정성껏 지도해주신 서지혜 교수님, 하은영 교수님, 박병덕 교수님께 감사드립니다. 또한 학위과정 중에 아낌없는 도움을 주고 격려해준 생화학교실 선생님들 모두 감사드립니다.

학위과정에서 연구뿐만 아니라 더 많은 것을 배웠습니다. 아직 많이 부족하지만 앞으로도 계속 정진하여 더 나은 사람이 될 수 있도록 노력하겠습니다.

마지막으로 항상 격려해주고 믿어주신 부모님께 감사드립니다. 아직 철없는 아들이지만 깊고 넓은 사랑으로 보듬어주신 부모님께 이 논문을 바칩니다.

2020년 8월

황 종 수

Table of Contents

1. Introduction	1
2. Materials and Methods	3
3. Results	8
4. Discussion	26
5. Summary	29
6. References	30
7. Abstract	36
8. 국문초록	38

List of Figures

Figure 1. Dose selection of METH in HBMECs	13
Figure 2. METH increases the BBB permeability in HBMECs	14
Figure 3. METH promotes ROS production in HBMECs	15
Figure 4. METH changes the cellular localization of junction proteins in HBMECs	16
Figure 5. METH induces cytoskeletal rearrangement in HBMECs	17
Figure 6. Dose selection of PBN and GKT136901 in HBMECs	18
Figure 7. PBN and GKT136901 inhibit METH-induced ROS generation in HBMECs	20
Figure 8. PBN and GKT136901 protect HBMECs against METH-induced BBB dysfunction	21
Figure 9. PBN and GKT136901 ameliorate METH-induced redistribution of junction proteins in HBMECs	23
Figure 10. PBN and GKT136901 attenuate METH-induced cytoskeletal	

rearrangement in HBMECs 25

1. Introduction

Methamphetamine (METH) is one of the most addictive psychostimulants. METH administration causes neurological and psychiatric disorders. It has been well-established that METH-induced neurotoxicity produces persistent damages to dopaminergic and serotonergic neurons in striatum, hippocampus and prefrontal cortex (1-3). However, the effects of METH on non-neuronal cells, including immune cells, endothelium, and glial cells remain unclear. Recently, several studies revealed that METH causes multiple detrimental effects on blood-brain barrier (BBB) function (4-6).

The BBB is a critical boundary between the blood and the brain to maintain the homeostasis of central nervous system (CNS). The BBB functions as a highly selective membrane barrier of endothelial cells that prevents the entry of large and potentially toxic molecules into the brain through tight junctions (TJs) and adherens junctions (AJs) (7,8) Indeed, BBB dysfunction has been reported in METH abuse (4,9,10). Several studies indicated that METH disrupts the junctions between brain endothelial cells, resulting in increased vascular permeability that leads to various brain pathological conditions, such as stroke, traumatic brain injury (TBI), and multiple sclerosis (11,12).

Although the molecular mechanisms of METH-induced BBB disruption have not been clarified, increased generation of reactive oxygen species (ROS) by METH has been considered as one of the main effects that promote BBB breakdown. Many earlier studies showed that abnormal ROS production alters the phenotype of endothelial cells that causes vascular hyper-permeability, resulting in brain edema and leukocyte infiltration from blood to the brain parenchyma (4,13-15). Therefore,

ROS inhibition could be considered as an efficient therapeutic strategy to protect BBB function against METH-abuse.

N-tert-butyl- α -phenylnitrone (PBN) is a ROS scavenger, reacting with ROS non-selectively as a potent free radical trapping agent. Unlike other free radical scavengers, PBN has a high level of BBB penetration. In line with this advantage, PBN has been shown to have neuroprotective properties on neuropathic pain behavior, TBI, and stroke (16,17).

GKT136901 is a highly selective small molecule inhibitor of NADPH oxidases (Nox) 1/4 (18), enzymes that generate ROS and are associated with brain injury. Compared to other Nox inhibitors, GKT136901 has good oral bioavailability and is well tolerated, suggesting that Nox 1/4 inhibition using GKT136901 could provide a safe and effective therapeutic approach for CNS diseases (19).

In this study, I examined the protective effect of PBN and GKT136901 against METH-induced BBB dysfunction. In primary human brain microvascular endothelial cells (HBMECs), PBN and GKT136901 improved the deleterious effect of METH on BBB function through inhibition of ROS production. Based on these studies, I suggest that PBN and GKT136901 could be utilized for BBB protection upon METH exposure as well as for the treatment of CNS diseases.

2. Materials and Methods

2.1. Materials and reagents:

GKT136901 (AOB6215) was purchased from Aobious (Gloucester, MA, USA). PBN (B7263) was purchased from Sigma Aldrich (St. Louis, MO, USA). METH was obtained from the Ministry of Food and Drug Safety of Korea. Cell counting kit-8 (CCK-8) was purchased from Dojindo (Kumamoto, Japan). Anti-ZO-1 (#40-2200) and anti-occludin (#33-1500) antibodies were purchased from Invitrogen (Carlsbad, CA, USA). Anti-VE-cadherin (ab33168) antibody was purchased from Abcam (Cambridge, UK). Anti- β -actin (sc-47778) antibody was purchased from Santa Cruz Biotechnology (Dallas, TX, USA).

2.2. Cell culture (*in vitro*):

HBMECs were purchased from Cell Systems (Kirkland, WA, USA) and cultured in EBMTM Basal Medium (Lonza, Walkersville, MD, USA) with EGMTM SingleQuotsTM SupplementPack (Lonza, Walkersville, MD, USA) and 100 U/mL penicillin and 100 mg/mL streptomycin. Cells were maintained at 37 °C in a humidified atmosphere containing 5% CO₂.

2.3. Cell viability assay:

Cell viability was assessed by CCK-8 assay according to the manufacturer's instructions (Dojindo, Kumamoto, Japan). HBMECs were seeded in a 96-well plate (2×10^4 cells per well). To select the

non-toxic condition, cells were treated with METH (0.1, 1 and 5 mM), PBN (50, 500 and 5000 nM) and GKT136901 (1, 10 and 100 μ M) (20–22). One mM METH, five hundred nM PBN, and ten μ M GKT136901 were chosen for the following experiments. For co-treatment of PBN and GKT136901 with METH, cells were pretreated with PBN and GKT136901 for 2 h before 1 mM METH treatment for 24 h. After treated with PBN and GKT136901, cells were incubated with CCK-8 reagent at 37 °C for 1 h. Absorbance was measured at 452 nm using a microplate reader (Tecan, Männedorf, Switzerland) (23).

2.4. BBB permeability assay:

Transwell chamber with pore size of 0.4 μ m (Corning, Tewksbury, MA, USA) was used for the permeability assay. HBMECs were seeded onto the collagen-coated membrane of the insert at a density of 4×10^4 cells per well and maintained in culture medium at 37 °C in a humidified chamber for 4 days until the cells were confluent. The cells were pretreated with PBN and GKT136901 for 2 h before METH treatment for 24 h. To assess the paracellular permeability, FITC-dextran (Sigma Aldrich, St. Louis, MO, USA) was added into the luminal chamber for 1 h at the end of the METH treatment (24,25). After incubation for 1 h, 60 μ L of medium was collected from the abluminal chamber and transferred into a black 96-well plate. Fluorescence intensity was measured by a microplate reader (480/520 nm).

2.5. Transendothelial electrical resistance (TEER)

measurement:

HBMECs were cultured onto the collagen-coated membrane of 24-transwell inserts. Cells were incubated for 4 days until 100% confluency. Cells were then treated with PBN and GKT136901 for 2 h, followed by METH treatment for 24 h. The TEER value was determined using STX2/chopstick electrodes connected to EVOM2 (World Precision Instruments, Sarasota, USA). Relative TEER values were calculated according to the manufacturer's instruction and expressed as TEER (%) (26).

2.6. ROS measurement:

HBMECs at a density of 2×10^4 cells per well were plated in 96-well plates. One mM METH was added to the cells for 30 and 60 min. To assess the inhibitory effect of PBN and GKT136901, cells were treated with PBN and GKT136901 for 2 h, and then exposed to METH for 60 min. After treatment, cells were washed with PBS and incubated with 5 μ M 2',7' - dichlorofluorescein diacetate (DCF-DA) for 30 min at 37 °C in a humidified chamber. Cells were then observed under a fluorescence microscope (Axio observer A1, Carl zeiss, Overkochen, Germany) and the intensity was measured by a microplate reader (485/535 nm) (27).

2.7. Immunocytochemistry and image analysis:

HBMECs were grown on collagen-coated coverslips in 24-well culture plates and treated with PBN and GKT136901 for 2 h, followed by METH treatment for 24 h. Cells were washed by PBS, and then fixed

with 4% paraformaldehyde (PFA) in PBS, followed by blocking with bovine serum albumin in PBS-T (0.05% Tween) for 1 h at room temperature (28). Cells were then incubated with the following primary antibodies overnight at 4 °C: anti-ZO-1 and anti-VE-cadherin. After rinsing in PBS, cells were incubated with anti-rabbit secondary antibodies conjugated with Alexa Fluor 488 or Alexa Fluor 568 (Invitrogen, Carlsbad, CA). Filamentous actin (F-actin) was stained using Alexa Fluor 488-conjugated phalloidin. Cells were then counterstained with 4',6-diamidino-2-phenylindole (DAPI) for nuclear labeling. After washing with PBS, coverslips were mounted on glass slides with aqueous mounting medium (Vector Laboratories, Burlingame, CA). Fluorescence images were captured using a confocal microscope (LSM5, Carl zeiss, Overkochen, Germany). Three-dimensional (3D) plot images were created from fluorescence images using the Interactive 3D Surface Plot plugin in Image J, where the luminance of an image is represented as height for the plot.

2.8. Western blot analysis:

HBMECs were seeded in 6-well plates at a density of 2×10^5 cells per well. Cells were treated with PBN and GKT136901 for 2 h before METH exposure for 24 h. Cells were then washed with PBS, harvested and lysed in radioimmunoprecipitation assay (RIPA) buffer (Thermo Fisher Scientific, Boston, MA, USA) with protease/phosphatase inhibitor cocktail. Protein concentration was determined by the BCA protein quantification assay. Total proteins (20 μ g) were separated by sodium dodecyl sulphate polyacrylamide gel electrophoresis (SDS-PAGE) (29). Immunoblotting was performed using the following primary antibodies:

anti-ZO-1, anti-VE-cadherin, anti-occludin, anti- β -actin, and horseradish peroxidase (HRP) - conjugated anti-rabbit secondary antibodies. Immunoblots were detected by electro-chemiluminescence (LAS-3000).

2.9. Statistical analysis:

Results are expressed as the mean \pm standard deviation (SD). *p* values were calculated by applying the two-tailed Student's *t*-test. Results with *p* value < 0.05 were considered as statistically significant.

3. Results

3.1. Dose selection of METH in HBMECs:

To determine the non-toxic METH concentration in HBMECs, cells were treated with different concentrations of METH ranging from 0.1 mM to 5.0 mM. After treatment for 24 h, cell viability was examined by CCK-8 assay. METH did not show a significant change in viability of HBMECs up to 1.0 mM, whereas 5.0 mM METH significantly decreased cell viability (Figure 1A&B). Based on these results, I chose 1.0 mM concentration of METH for the subsequent experiments.

3.2. METH increases the BBB permeability in HBMECs:

To assess the BBB permeability, I performed *in vitro* permeability assay using 24-transwell cell culture inserts. I first investigated paracellular permeability of HBMECs using FITC-dextran (70 kDa). As shown in Figure 2A&B, METH increased the influx of FITC-dextran from luminal to abluminal chamber. Next, I measured TEER of the confluent monolayer of HBMECs after METH treatment. METH significantly reduced the TEER of HBMEC monolayer (Figure 2C&D). These data suggest that METH decreases the barrier function of HBMECs.

3.3. METH promotes ROS production in HBMECs:

Since numerous previous studies have shown that METH induces oxidative stress in various types of brain cells, including neurons, glia, and cerebral endothelium, I examined ROS generation in METH-treated HBMECs using DCF-DA. As shown in Figure 3A&B, METH significantly increased ROS production in HBMECs. These results indicate that METH elevates intracellular ROS levels in HBMECs.

3.4. METH changes the cellular localization of junction proteins in HBMECs:

Since BBB function of endothelial cells is mainly modulated by TJ and AJ proteins (30), I examined the effect of METH on junction proteins in HBMECs using immunostaining. As shown in Figure 4, METH exposure disrupted TJ proteins (ZO-1 and Claudin-5) as well as AJ protein (VE-cadherin) in HBMECs. METH also induced redistribution of junction proteins through changing the cellular localization from membrane to cytosol in HBMECs (Figure 4). This finding suggests that METH disrupts BBB structure between cells through translocation of junction proteins from membrane to cytosol.

3.5. METH induces cytoskeletal rearrangement in HBMECs:

I observed that METH strongly changed the cellular morphology of HBMECs. Compared to untreated group, METH-exposed HBMECs exhibited linear and elongated structure (Figure 5A). Cytoskeleton is a critical modulator of cellular morphology (31). Therefore, I checked the

formation of F-actin stress fiber by phalloidin staining. As shown in Figure 5B, METH-treated HBMECs formed F-actin stress fibers in all doses. These results indicate that METH induces cytoskeletal reorganization through stress fiber formation.

3.6. Dose selection of PBN and GKT136901 in HBMECs:

To determine the non-toxic concentration of PBN and GKT136901, I treated PBN and GKT136901 for 24 h at indicated concentrations. As shown in Figure 6A&B, cell viability after treatment of PBN and GKT136901 did not show considerable changes up to 500 nM PBN and 10 μ M GKT136901, respectively. However, 5000 nM PBN and 100 μ M GKT136901 showed apparent decreases in cell viability of HBMECs. Based on these results, cells were treated with 500 nM PBN and 10 μ M GKT136901 for the following experiments.

Next, I checked the effect of co-treatment of PBN and GKT136901 with METH on cell viability. HBMECs were treated with PBN and GKT136901 for 2 h before METH exposure for 24 h. As shown in Figure 6C, co-treatment did not affect the cell viability in HBMECs. In accordance with this result, this co-treatment condition was applied to the subsequent experiments.

3.7. PBN and GKT136901 inhibit METH-induced ROS generation in HBMECs:

To investigate the protective effect of PBN and GKT136901 on METH-induced ROS formation, HBMECs were treated with PBN and GKT136901 prior to METH treatment. As expected, PBN and

GKT136901 significantly abolished ROS generation stimulated by METH treatment (Figure 7A&B). The results indicate that METH-induced elevation of ROS levels is diminished by PBN and GKT136901.

3.8. PBN and GKT136901 protect HBMECs against METH-induced BBB dysfunction

Next, I examined whether PBN and GKT136901 could protect HBMECs against METH-induced BBB dysfunction. BBB function in HBMECs was analyzed by paracellular permeability and TEER assay. As shown in Figure 8A, monolayer permeability of HBMECs was highly increased upon METH treatment compared to the untreated group. However, PBN and GKT136901 abolished this perturbation in endothelial permeability. Consistent with the FITC-dextran permeability assay, METH decreased TEER value of HBMECs monolayer, and this effect was eliminated upon PBN and GKT136901 treatment (Figure 8B). These results indicate the protective effect of PBN and GKT136901 in METH-induced BBB dysfunction.

3.9. PBN and GKT136901 ameliorate METH-induced redistribution of junction proteins in HBMECs:

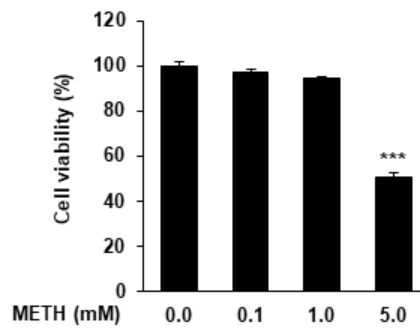
To evaluate the expressions of junction proteins such as ZO-1, VE-cadherin, and occludin in HBMECs, cells were treated with METH alone and in combination with PBN and GKT136901. The expression levels of TJ and AJ proteins were detected by western blotting. As shown in Figure 9A, total protein expression levels of ZO-1, VE-cadherin, and occludin were not altered when cells were treated

with PBN and GKT136901 before METH treatment. Next, the subcellular localization of TJ and AJ protein was analyzed by immunocytochemistry. Under normal conditions, ZO-1 and VE-cadherin were mainly localized in the cell membrane. However, after HBMECs were treated with METH, ZO-1 and VE-cadherin were translocated to the cytoplasm. However, METH-induced translocation of these junction proteins was ameliorated upon treatment of PBN and GKT136901 (Figure 9B&C). This observation is consistent with the result of cellular permeability assay. These data suggest that PBN and GKT136901 attenuate METH-induced BBB dysfunction through the modulation of subcellular distribution of TJ and AJ proteins.

3.10. PBN and GKT136901 attenuate METH-induced cytoskeletal rearrangement in HBMECs:

Finally, I examined the effect of PBN and GKT136901 on cytoskeletal rearrangement. METH altered cellular morphology and this change was inhibited by PBN and GKT136901 treatment in HBMECs (Figure 10A). Consistent with this result, PBN and GKT136901 prevented the formation of stress fibers induced by METH (Figure 10B). These results indicate that PBN and GKT136901 preserve cell morphology of METH-exposed HBMECs via structural modulation of cytoskeleton.

A



B

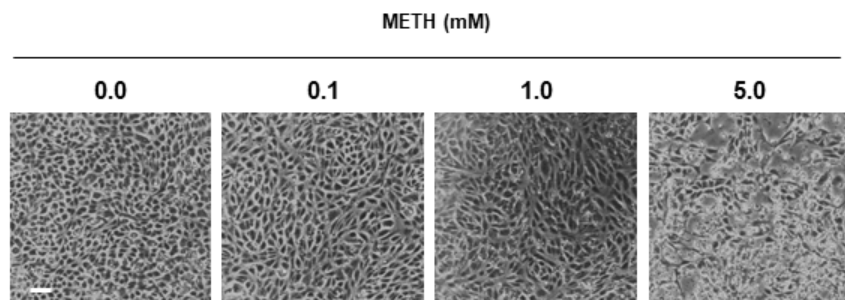


Figure 1. Dose selection of METH in HBMECs (A) Cell viability of METH-treated HBMECs. Cells were treated with indicated concentrations of METH (0.1, 1.0 and 5.0 mM) for 24 h. (B) The morphology of the cells were observed under the light microscope after METH treatment for 24 h (scale bar: 100 μ m). The graph is presented as mean \pm SD of three individual experiments. *** $p < 0.001$.

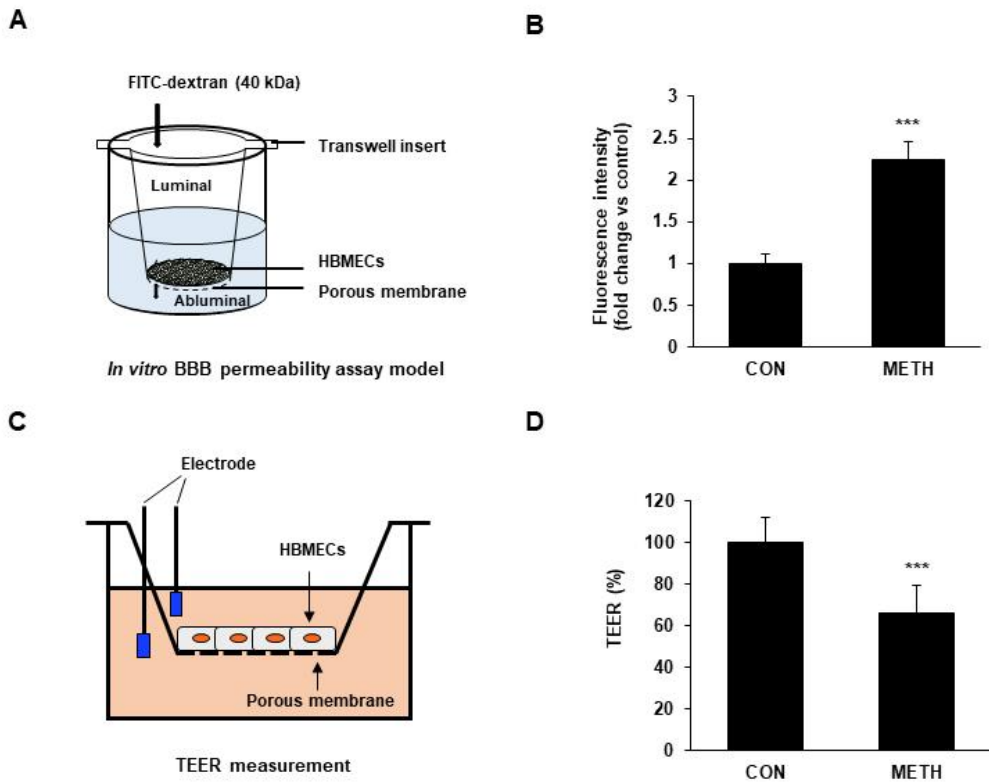


Figure 2. METH increases the BBB permeability in HBMECs. (A&B) FITC-dextran (70 kDa) was added into the luminal chamber after 1 mM METH treatment for 24 h in HBMECs. The fluorescence intensity was measured by spectrophotometry (480/520 nm). (C&D) Monolayer integrity of HBMECs was measured with TEER value. All data are presented as mean \pm SD of three individual experiments. *** $p < 0.001$.

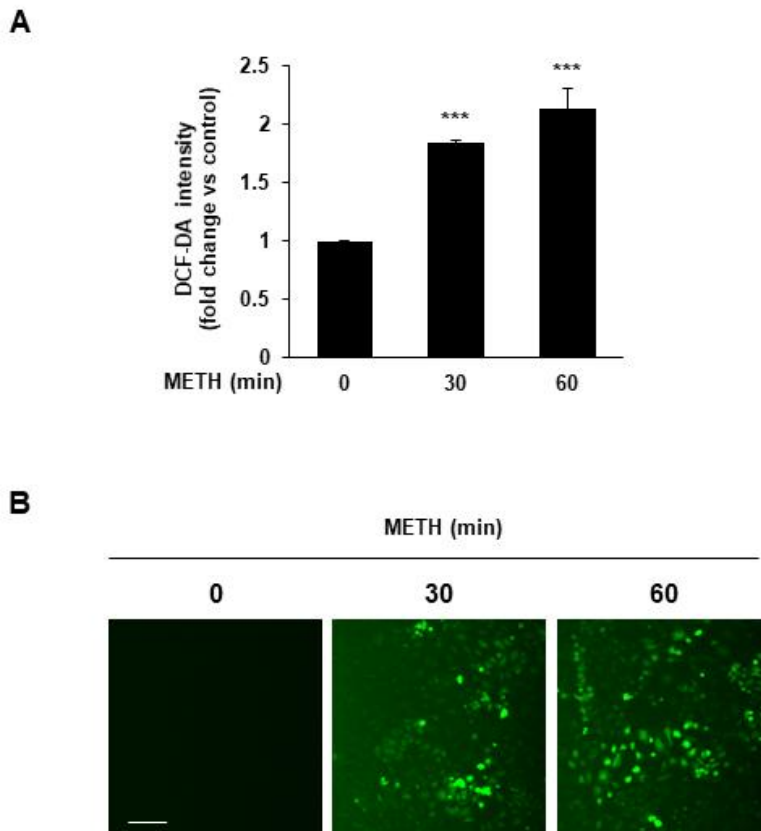


Figure 3. METH promotes ROS production in HBMECs. (A) HBMECs were treated with 1 mM METH for 30 and 60 min. After treatment of METH, cells were incubated with 5 μ M DCF-DA, followed by measurement of fluorescence at 485/535 nm. (B) The DCF-DA staining images were captured by fluorescence microscopy after METH treatment for 30 and 60 min (scale bar: 20 μ m). The graph is presented as mean \pm SD of three individual experiments. *** $p < 0.001$.

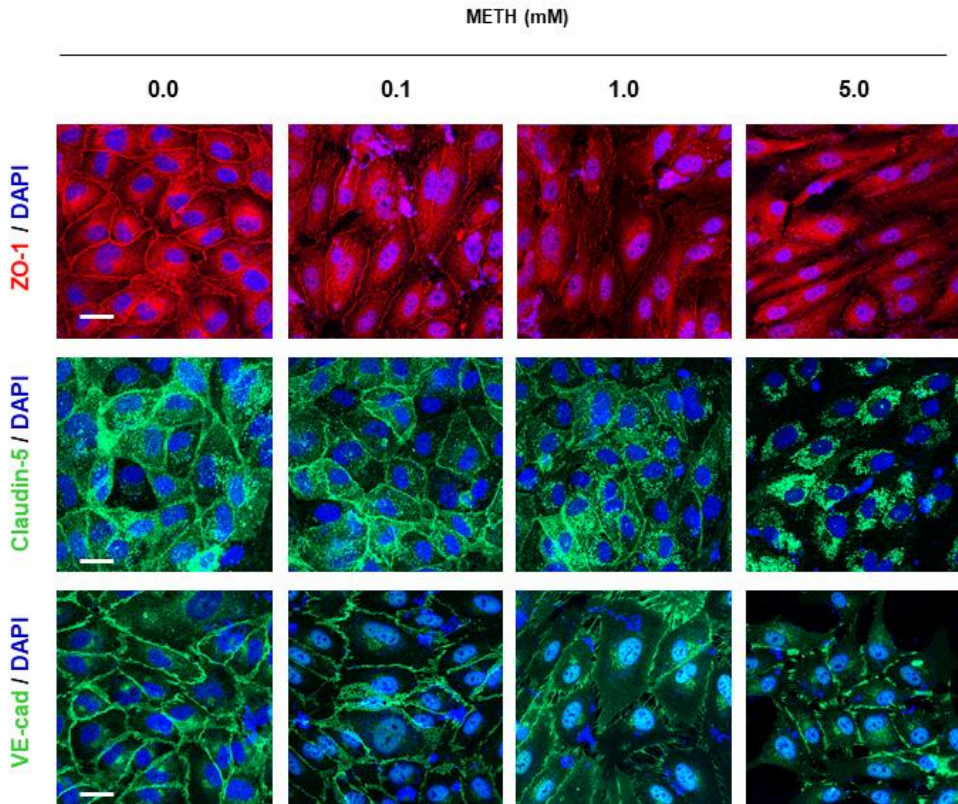


Figure 4. METH changes the cellular localization of junction proteins in HBMECs. Indicated concentrations of METH (0.1, 1.0 and 5.0 mM) were treated to HBMECs for 24 h. Cells were then immunostained with ZO-1 (red), Claudin-5 (green), and VE-cadherin (green). Nuclear staining was performed using DAPI (scale bar: 20 μ m). Fluorescence images are visualized using a confocal microscope. Representative images were from three individual experiments.

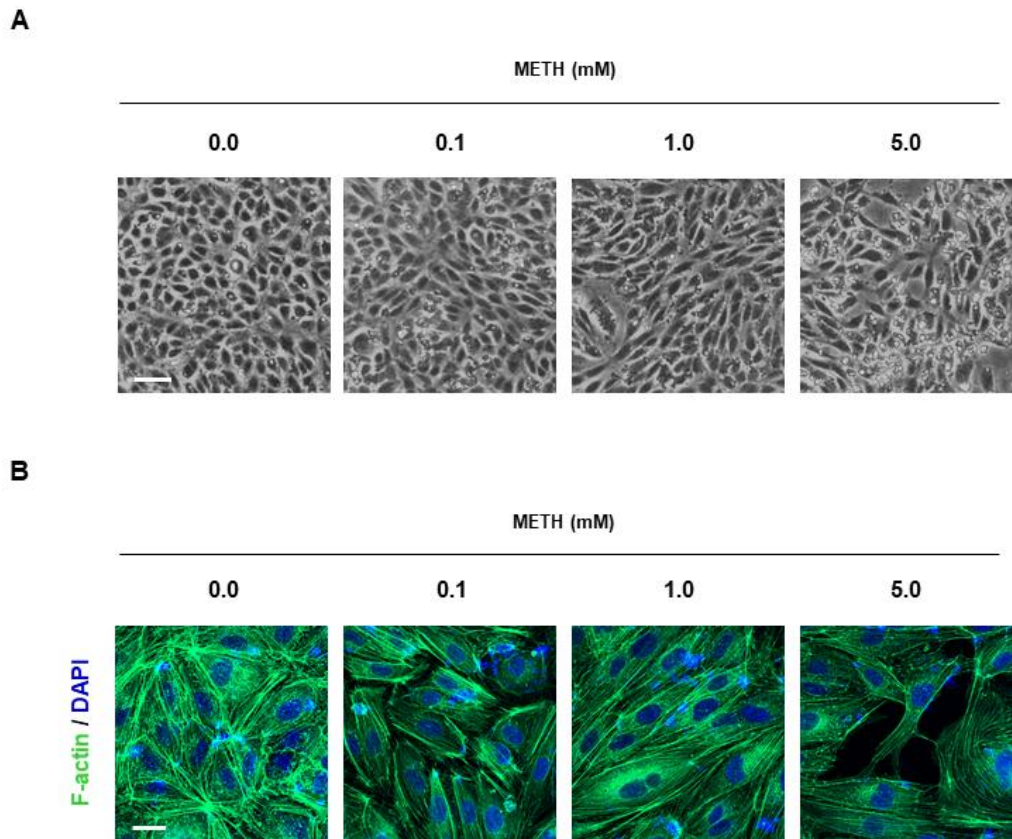
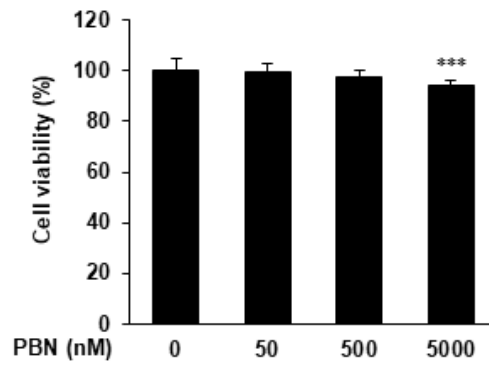
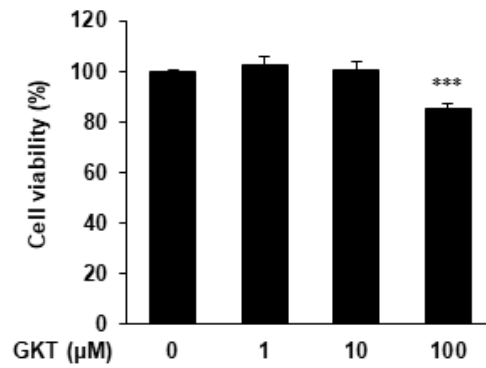


Figure 5. METH induces cytoskeletal rearrangement in HBMECs. (A) The light microscopic pictures were captured after cells were treated with indicated concentrations of METH (0.1, 1 and 5 mM) for 24 h (scale bar: 100 μ m). (B) HBMECs were treated with METH at indicated concentrations for 24 h, followed by incubation with phalloidin for F-actin staining (scale bar: 20 μ m). Stress fibers were analyzed under a confocal microscope. Representative images were from three individual experiments.

A



B



C

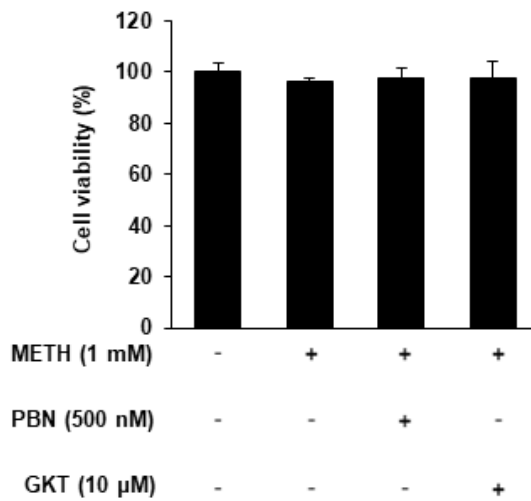


Figure 6. Dose selection of PBN and GKT136901 in HBMECs (A&B) HBMECs were incubated with PBN (50, 500 and 5000 nM) and GKT136901 (1, 10 and 100 μ M) for 24 h. Cell viability was measured using CCK-8 reagent at 452 nm. (C) Cells were pretreated with 500 nM PBN and 10 μ M GKT136901 for 2 h, followed by treatment of 1 mM METH for 24 h. After METH treatment, cell viability was determined by CCK-8 assay. All data are presented as mean \pm SD of three individual experiments. *** $p < 0.001$.

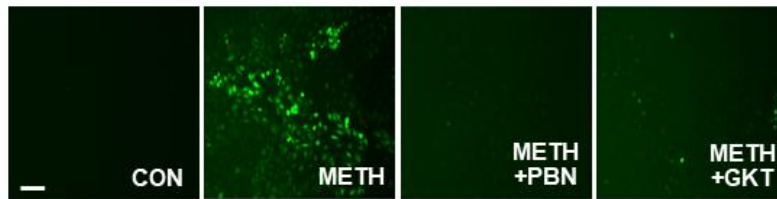
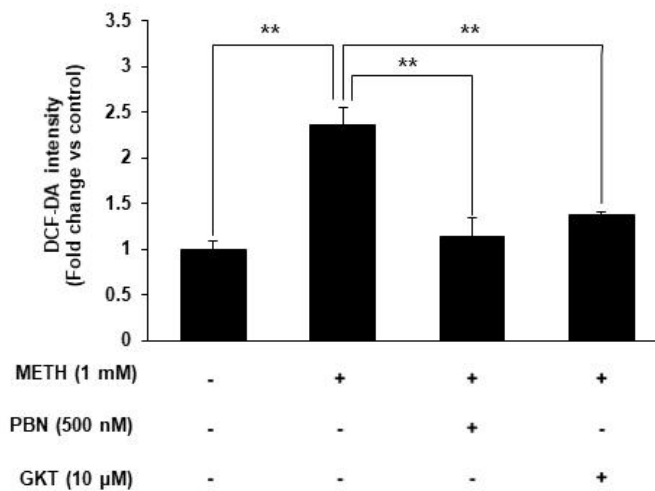
A

B


Figure 7. PBN and GKT136901 inhibit METH-induced ROS generation in HBMECs. (A) HBMECs were pretreated with 500 nM PBN and 10 μM GKT136901 for 2 h before 1 mM METH treatment for 24 h. ROS production was observed under fluorescence microscopy. Fluorescence images of DCF-DA were captured by fluorescence microscopy (scale bar: 100 μm). (B) Cells were exposed to 1 mM METH after treatment of 500 nM PBN and 10 μM GKT136901. Intracellular ROS levels were quantified with measurement of DCF-DA intensity (485/535 nm). The graph is presented as mean ± SD of three individual experiments. ** $p < 0.01$.

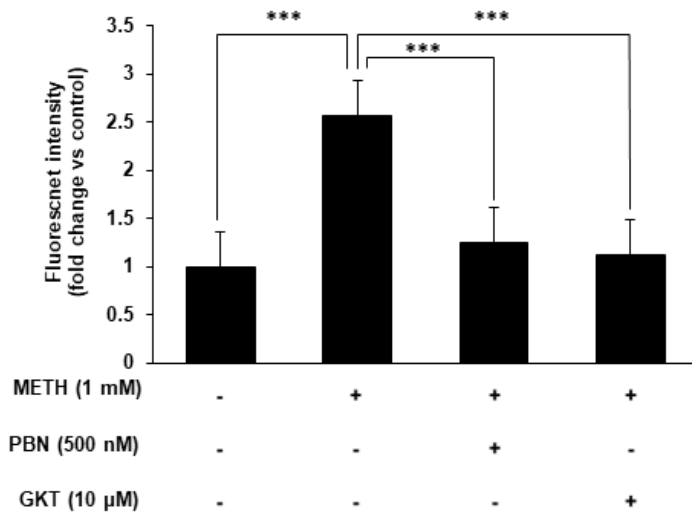
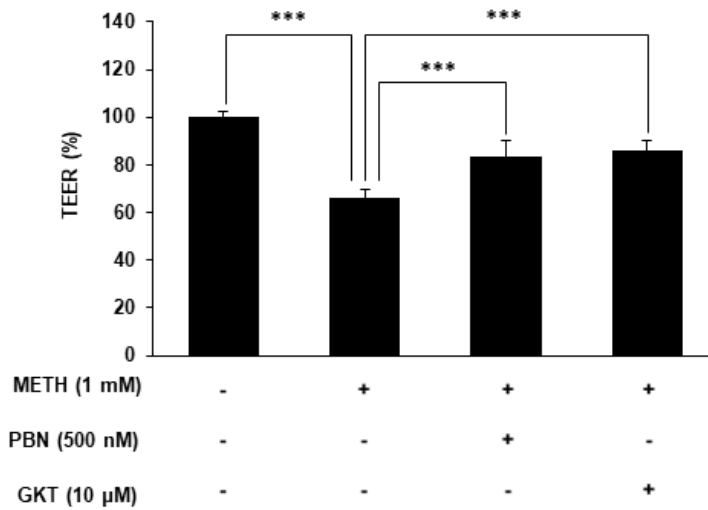
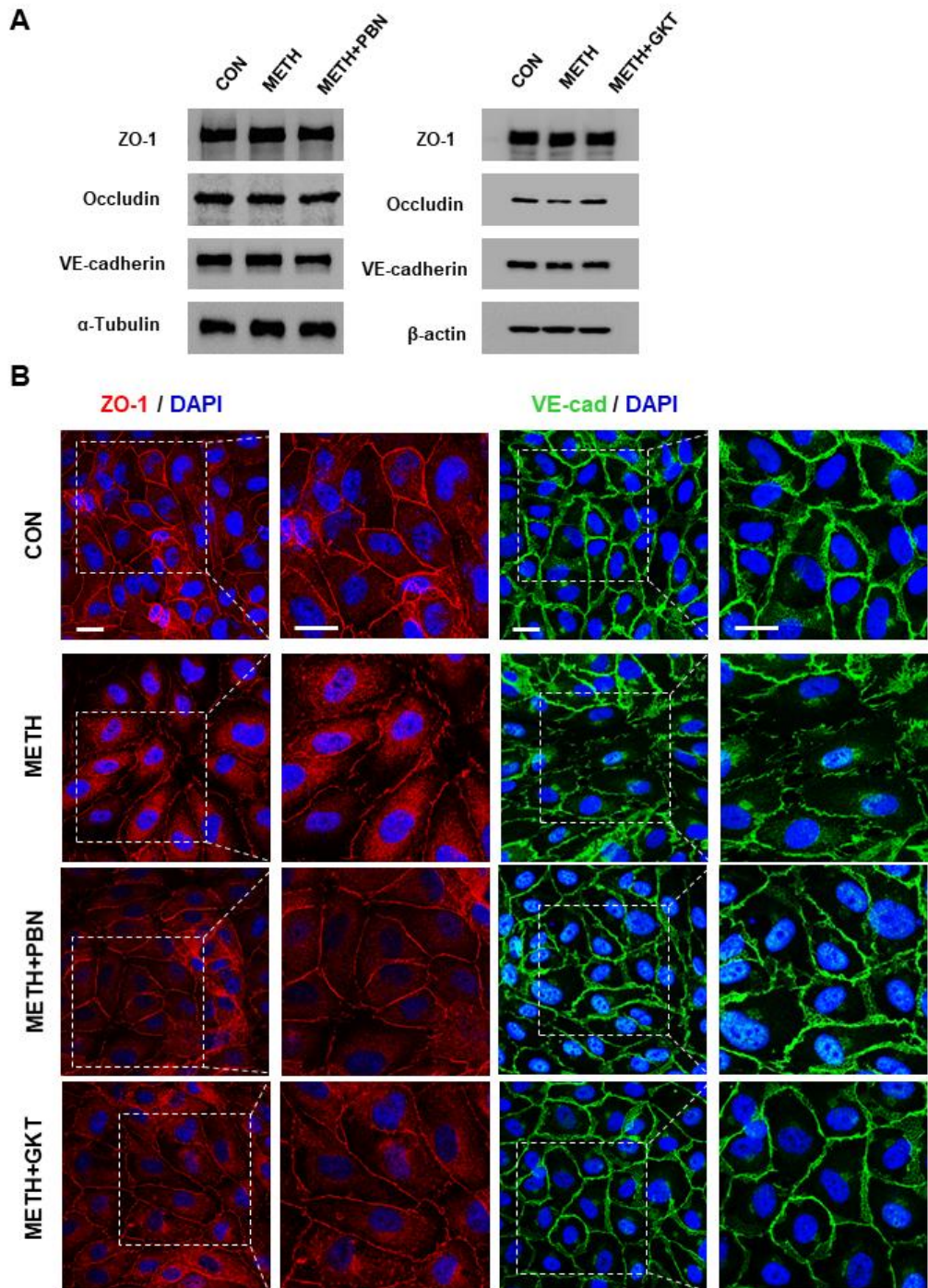
A

B


Figure 8. PBN and GKT136901 protect HBMECs against METH-induced BBB dysfunction. (A) HBMECs were pretreated with 500 nM PBN and 10 μ M GKT136901, followed by 1 mM METH treatment for 24 h. Fluorescence intensity of FITC-dextran (70 kDa) from abluminal chamber was measured by a microplate

reader (480/520 nm). (B) TEER values of HBMECs monolayer were measured after pretreatment of 500 nM PBN and 10 μ M GKT136901 before 1 mM METH treatment. All data are presented as mean \pm SD of three individual experiments. ** p < 0.01, *** p < 0.001.



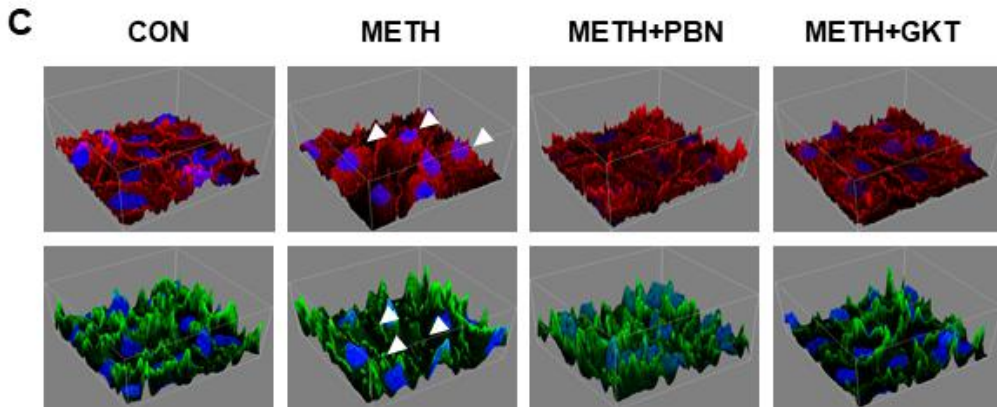


Figure 9. PBN and GKT136901 ameliorate METH-induced redistribution of junction proteins in HBMECs. (A) HBMECs were treated with 1 mM METH for 24 h after pretreatment with 500 nM PBN and 10 μ M GKT136901 for 2 h. Total protein expression levels of ZO-1, occludin, and VE-cadherin were analyzed by western blotting. (B) Cells were stained for ZO-1 (red) and VE-cadherin (green). Nuclear staining was performed using DAPI (scale bar: 20 μ m). Stained junction proteins were visualized using a confocal microscope. (C) Three-dimensional plot images were generated from the area indicated by white square dashes in (B). Arrow heads indicate translocation of junction proteins. Representative images were from three individual experiments.

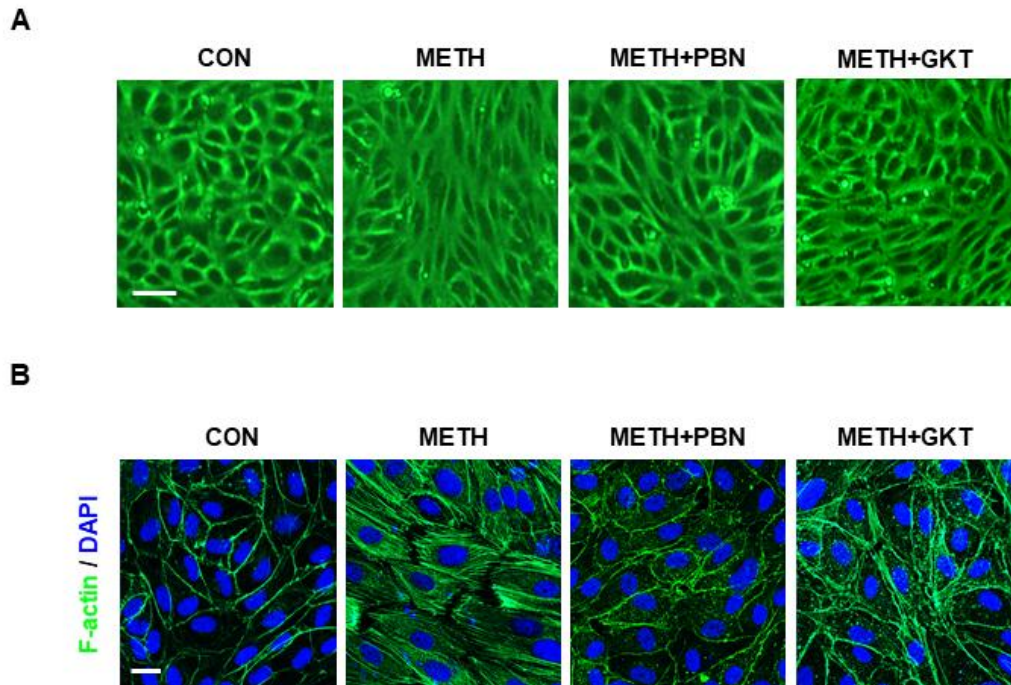


Figure 10. PBN and GKT136901 attenuate METH-induced cytoskeletal rearrangement in HBMECs. (A) HBMECs were treated with 500 nM PBN and 10 μ M GKT136901 for 2 h, followed by 1 mM METH treatment for 24 h. Cell morphology was analyzed under a microscope (scale bar: 100 μ m). (B) F-actin were immunostained with phalloidin. The nuclei were labeled with DAPI (scale bar: 20 μ m). Fluorescence images were captured by a confocal microscope. Representative images were from three individual experiments.

4. Discussion

The present study provides a protective effect of PBN and GKT136901 against METH-induced BBB impairment. PBN and GKT136901, ROS scavenger and specific Nox 1/4 inhibitor, respectively, showed great efficacy in neurodegenerative diseases as well as vascular dysfunction by inhibiting ROS-induced oxidative stress (16-18). ROS are well-known factors participating in many pathological conditions. Previous studies reported that induction of ROS by METH in brain and endothelial cells results in various brain diseases (4,32-34). Hence, I hypothesized that inhibition of METH-induced ROS accumulation through PBN and GKT136901 treatment may have protective effects on BBB function.

Excessive ROS have been proposed to be responsible for BBB dysfunction by damaging the BBB structure (14,15). The present study reveals that METH increases the paracellular permeability and decreases the monolayer integrity of HBMECs through excessive ROS production (Figure 2&3). Previous studies have suggested that ROS inhibition provides neuroprotective effect and endothelial dysfunction (35). Our results demonstrated that PBN and GKT136901 showed protective effects on METH-induced BBB leakage through inhibition of excessive ROS generation upon METH treatment in HBMECs (Figure 7&8). These results were in accordance with previous studies that showed PBN and GKT136901 inhibited ROS-induced oxidative stress that contributes development of vascular dysfunction in preclinical studies

(17,18).

TJs and AJs that are linked to the cytoskeleton are major components of BBB structure (8). The current study showed that METH disrupted TJ and AJ proteins in HBMECs. However, METH did not affect the expressions of endothelial junction proteins but changed the subcellular localization of junction proteins from membrane to cytoplasm (Figure 4). Previous studies have reported that junction proteins anchored to the actin cytoskeleton are disassembled by stress fiber formation, facilitating internalization of junction proteins (36). Our results demonstrated that METH treatment induced generation of excessive stress fibers, resulting in phenotype alterations in HBMECs (Figure 5). ROS decrease the BBB integrity via actin cytoskeletal reorganization and redistribution of junction proteins (37). By preserving BBB integrity after METH treatment, PBN and GKT136901 ameliorated METH-induced internalization of TJ and AJ proteins through inhibition of stress fibers formed by METH treatment (Figure 9&10). Consequently, these observations reveal that PBN and GKT136901 attenuated METH-induced formation of stress fibers, there by redistribution of junction proteins in HBMECs.

Although this study demonstrated the protective effects of PBN and GKT136901 against METH exposure, the molecular mechanism under METH-induced BBB dysfunction remain unclear. Since present study focused on the evaluation of the effects of PBN and GKT136901 on BBB protection, further studies are warranted to identify the signaling pathway in METH-induced BBB disruption. In addition, previous *in vivo* studies revealed that METH-induced oxidative stress disrupts BBB

(4,38), it will be interesting to test the efficacy of PBN and GKT136901 in *in vivo* studies.

In conclusion, this study demonstrated that PBN and GKT136901 attenuated METH-induced BBB dysfunction in HBMECs. Thus, PBN and GKT136901 could be promising therapeutic reagents for the treatment of METH-induced BBB impairment.

5. Summary

In this study, the protective roles of PBN and GKT136901 against METH-induced BBB dysfunction was investigated. The results demonstrated that METH induced BBB disruption by enhancing ROS production. However, PBN and GKT136901 remarkably counteracted the harmful effects of METH on BBB function through inhibiting ROS generation. Furthermore, PBN and GKT136901 protected the BBB from METH-induced formation of stress fibers, there by preventing junctional protein redistribution from METH exposure. Taken together, this study suggests that PBN and GKT136901 could be considered as therapeutic reagents for protecting BBB function against METH exposure.

References

1. Seiden LS, Commins DL, Vosmer G, Axt K, Marek G: Neurotoxicity in dopamine and 5-hydroxytryptamine terminal fields: a regional analysis in nigrostriatal and mesolimbic projections. *Ann N Y Acad Sci* 1988; 537: 161-72.
2. Gold MS, Kobeissy FH, Wang KK, Merlo LJ, Bruijnzeel AW, Krasnova IN, et al.: Methamphetamine- and trauma-induced brain injuries: comparative cellular and molecular neurobiological substrates. *Biol Psychiatry* 2009; 15: 118-27.
3. Krasnova IN, Cadet JL: Methamphetamine toxicity and messengers of death. *Brain Res Rev* 2009; 60: 379-407.
4. Sajja RK, Rahman S, Cucullo L: Drugs of abuse and blood-brain barrier endothelial dysfunction: A focus on the role of oxidative stress. *J Cereb Blood Flow Metab* 2016; 36: 539-54.
5. Ramirez SH, Potula R, Fan S, Eidem T, Papugani A, Reichenbach N, et al.: Methamphetamine disrupts blood-brain barrier function by induction of oxidative stress in brain endothelial cells. *J Cereb Blood Flow Metab* 2009; 29: 1933-45.
6. Park M, Hennig B, Toborek M. Methamphetamine alters occludin expression via NADPH oxidase-induced oxidative insult and intact caveolae: *J Cell Mol Med* 2012; 16: 362-75.

7. Abbott NJ, Patabendige AA, Dolman DE, Yusof SR, Begley DJ: Structure and function of the blood-brain barrier. *Neurobiol Dis* 2010; 37: 13-25.
8. Daneman R, Prat A: The blood-brain barrier. *Cold Spring Harb Perspect Biol* 2015; 7: a020412.
9. Lappin JM, Darke S, Farrell M: Stroke and methamphetamine use in young adults: a review. *J Neurol Neurosurg Psychiatry* 2017; 88: 1079-91.
10. Northrop NA, Yamamoto BK: Methamphetamine effects on blood-brain barrier structure and function. *Front Neurosci* 2015; 9: 69.
11. Lee HS, Han J, Bai HJ, Kim KW: Brain angiogenesis in developmental and pathological processes: regulation, molecular and cellular communication at the neurovascular interface. *FEBS J* 2009; 276: 4622-35.
12. Arai K, Jin G, Navaratna D, Lo EH: Brain angiogenesis in developmental and pathological processes: neurovascular injury and angiogenic recovery after stroke. *FEBS J* 2009; 276: 4644-52.
13. Jayaraj RL, Azimullah S, Beiram R, Jalal FY, Rosenberg GA: Neuroinflammation: friend and foe for ischemic stroke. *J Neuroinflammation* 2019; 16: 142.

14. Himadri P, Kumari SS, Chitharanjan M, Dhananjay S: Role of oxidative stress and inflammation in hypoxia-induced cerebral edema: a molecular approach. *High Alt Med Biol* 2010; 11: 231-44.
15. Aitken RJ, Baker MA: Oxidative stress, spermatozoa and leukocytic infiltration: relationships forged by the opposing forces of microbial invasion and the search for perfection. *J Reprod Immunol* 2013; 100: 11-9.
16. Kim HK, Zhang YP, Gwak YS, Abdi S: Phenyl N-tert-butyl nitron, a free radical scavenger, reduces mechanical allodynia in chemotherapy-induced neuropathic pain in rats. *Anesthesiology* 2010; 112: 432-9.
17. Marklund N, Lewander T, Clausen F, Hillered L: Effects of the nitron radical scavengers PBN and S-PBN on in vivo trapping of reactive oxygen species after traumatic brain injury in rats. *J Cereb Blood Flow Metab* 2001; 21: 1259-67.
18. Teixeira G, Szyndralewicz C, Molango S, Carnesecchi S, Heitz F, Wiesel P, et al.: Therapeutic potential of NADPH oxidase 1/4 inhibitors. *Br J Pharmacol.* 2017; 174: 1647-69.
19. Laleu B, Gaggini F, Orchard M, Fioraso-Cartier L, Cagnon L, Houngninou-Molango, et al.: First in class, potent, and orally bioavailable NADPH oxidase isoform 4 (Nox4) inhibitors for the treatment of idiopathic pulmonary fibrosis. *J Med Chem* 2010; 11; 7715-30.

20. Qie X, Wen D, Guo H, Xu G, Liu S, Shen Q, et al.: Endoplasmic reticulum stress mediates methamphetamine-induced blood-brain barrier damage. *Front Pharmacol* 2017; 8: 639.
21. Wong HS, Benoit B, Brand MD: Mitochondrial and cytosolic sources of hydrogen peroxide in resting C2C12 myoblasts. *Free Radic Biol Med* 2019; 130: 140-50.
22. Schulz JB, Weller M, Klockgether T: Potassium deprivation-induced apoptosis of cerebellar granule neurons: a sequential requirement for new mRNA and protein synthesis, ICE-like protease activity, and reactive oxygen species. *J Neurosci* 1996; 16: 4696-706.
23. Liu HQ, An YW, Hu AZ, Li MH, Wu JL, Liu L, et al.: Critical roles of the PI3K-Akt-mTOR signaling pathway in apoptosis and autophagy of astrocytes induced by methamphetamine. *Open Chem* 2019; 17; 96-104.
24. Shi Y, Jiang X, Zhang L, Pu H, Hu X, Zhang W, et al.: Endothelium-targeted overexpression of heat shock protein 27 ameliorates blood-brain barrier disruption after ischemic brain injury. *Proc Natl Acad Sci U S A* 2017; 114: E1243-52.
25. Martins T, Burgoyne T, Kenny BA, Hudson N, Futter CE, Ambrósio AF, et al.: Methamphetamine-induced nitric oxide promotes vesicular transport in blood-brain barrier endothelial cells. *Neuropharmacology*. 2013; 65: 74-82.
26. Parikh NU, Aalinkeel R, Reynolds JL, Nair BB, Sykes DE, Mammen

- MJ, et al.: Galectin-1 suppresses methamphetamine induced neuroinflammation in human brain microvascular endothelial cells: Neuroprotective role in maintaining blood brain barrier integrity. *Brain Res* 2015; 1624: 175-87.
27. Sivandzade F, Cucullo L: Assessing the protective effect of rosiglitazone against electronic cigarette/tobacco smoke-induced blood-brain barrier impairment. *BMC Neurosci* 2019; 20: 15.
28. Shi Y, Zhang L, Pu H, Mao L, Hu X, Jiang X, et al.: Rapid endothelial cytoskeletal reorganization enables early blood-brain barrier disruption and long-term ischaemic reperfusion brain injury. *Nat Commun* 2016; 7: 10523.
29. Sivandzade F, Cucullo L: Anti-diabetic countermeasures against tobacco smoke-dependent cerebrovascular toxicity: use and effect of rosiglitazone. *Int J Mol Sci* 2019; 20: 4225.
30. Seo JH, Guo S, Lok J, Navaratna D, Whalen MJ, Kim KW, et al.: Neurovascular matrix metalloproteinases and the blood-brain barrier. *Curr Pharm Des* 2012; 18:3645-8.
31. Fletcher DA, Mullins RD: Cell mechanics and the cytoskeleton. *Nature* 2010; 463: 485-92.
32. Peerzada H, Gandhi JA, Guimaraes AJ, Nosanchuk JD, Martinez LR: Methamphetamine administration modifies leukocyte proliferation and cytokine production in murine tissues. *Immunobiology* 2013; 218: 1063-8.

33. Castellano P, Nwagbo C, Martinez LR, Eugenin EA: Methamphetamine compromises gap junctional communication in astrocytes and neurons. *J Neurochem* 2016; 137: 561-75.
34. Krasnova IN, Cadet JL: Methamphetamine toxicity and messengers of death. *Brain Res Rev* 2009; 60: 379-407.
35. Kim H, Yun J, Kwon SM: Therapeutic Strategies for Oxidative Stress-Related Cardiovascular Diseases: Removal of Excess Reactive Oxygen Species in Adult Stem Cells. *Oxid Med Cell Longev* 2016; 2016: 2483163.
36. Stamatovic SM, Keep RF, Wang MM, Jankovic I, Andjelkovic AV: Caveolae-mediated internalization of occludin and claudin-5 during CCL2-induced tight junction remodeling in brain endothelial cells. *J Biol Chem* 2009; 284: 19053-19066.
37. Schreibelt G, Kooij G, Reijkerkerk A, van Doorn R, Gringhuis SI, van der Pol S, et al.: Reactive oxygen species alter brain endothelial tight junction dynamics via RhoA, PI3 kinase, and PKB signaling. *The FASEB Journal* 2017; 21: 3666-3676.
38. Toborek M, Seelbach MJ, Rashid CS, András IE, Chen L, Park M, et al.: Voluntary exercise protects against methamphetamine-induced oxidative stress in brain microvasculature and disruption of the blood-brain barrier. *Mol Neurodegener* 2013; 8: 22.

Protective Roles of PBN and GKT136901 in METH-Induced BBB Dysfunction

Hwang, Jong Su

Department of biochemistry

Graduate School

Keimyung University

(Supervised by Professor Seo, Ji Hae)

(Abstract)

Methamphetamine (METH) is a strong psychostimulant abused worldwide. While most studies have focused on the neurotoxic effects of METH, METH-induced cerebrovascular dysfunction has recently drawn attention as an important facet of METH-related pathophysiology. In this study, I investigated the protective roles of PBN and GKT136901 against METH-induced blood-brain barrier (BBB) dysfunction. In primary human brain microvascular endothelial cells (HBMECs), METH treatment promotes reactive oxygen species (ROS) generation in HBMECs and METH-induced ROS production was inhibited by PBN and GKT136901 treatment. In addition, METH increased permeability of HBMECs monolayer and this effect was abolished by PBN and GKT136901 treatment. Following METH exposure, the proteins zonula

occludens-1 (ZO-1) and vascular endothelial cadherin (VE-cadherin) were translocated from the cell membrane to the cytoplasm, which were ameliorated upon PBN and GKT136901 treatment. METH induced the cellular morphology change and stress fiber formation and this change was prevented by PBN and GKT136901 treatment. Taken together, this study suggest that PBN and GKT136901 could be promising therapeutic reagents against METH-induced BBB dysfunction.

메스암페타민에 의한 뇌혈관장벽 장애에 대한

PBN과 GKT136901의 역할

황 종 수

계명대학교 대학원

의학과 생화학 전공

(지도교수 서 지 혜)

(초록)

메스암페타민은 세계적으로 남용되는 강력한 중추신경흥분제이다. 그동안 대부분의 연구들이 메스암페타민의 신경독성에 집중되어 있었다. 최근 메스암페타민에 의한 뇌혈관장애는 병태생리학의 중요한 부분으로서 주목받기 시작했다. 본 연구에서는 메스암페타민에 의한 뇌혈관장벽 장애에 대한 PBN과 GKT136901의 보호적인 역할에 대해 조사하였다. 뇌혈관내피세포에서 메스암페타민은 활성산소종 발생을 촉진시켰으며, 이러한 메스암페타민에 의한 활성산소종 발생은 PBN과 GKT136901에 의해 저해되었다. 또한 메스암페타민에 의해 증가되었던 뇌혈관내피세포 단층의 투과성이 PBN과 GKT136901에 의해 다시 감소하였고, 세포막에서 세포질로의 세포연접 단백질 위치변화가 PBN과 GKT136901 처리에 의해 완화되었다. 메스암페타민은 뇌혈관내피세포의 형태를 변화시키고 스트레스 섬유를 유발하였으나 PBN과 GKT136901은 이러한 변화를 저해하였다. 결과적으로 본 연구는

PBN과 GKT136901의 메스암페타민에 의한 뇌혈관장벽장애 치료제로서 활용 가능성을 제시한다.